

## Calculation of core-hole excitonic features on Al $L_{23}$ -edge x-ray-absorption spectra of $\alpha$ -Al<sub>2</sub>O<sub>3</sub>

Isao Tanaka and Hirohiko Adachi

*Department of Materials Science and Engineering, Kyoto University, Sakyo, Kyoto 606-01 Japan*

(Received 11 March 1996)

We carry out first-principles molecular-orbital calculations for model clusters composed of 21 to 41 atoms with and without inclusion of a core hole. The strongest peak that appears near the Al  $L_{23}$ -edge x-ray-absorption spectrum and electron energy-loss spectrum of  $\alpha$ -Al<sub>2</sub>O<sub>3</sub> is found to originate from the presence of a core hole. Such an effect is less significant in MgO and  $\alpha$ -quartz (SiO<sub>2</sub>). The cation-cation overlap population in the lowest unoccupied molecular orbital (LUMO) is found to be exceptionally strong at one of the Al-Al bonds in  $\alpha$ -Al<sub>2</sub>O<sub>3</sub> because of its short Al-Al bond length. The LUMO strongly localizes when the core hole is introduced. [S0163-1829(96)04331-7]

### INTRODUCTION

Recently, both near-edge x-ray-absorption fine structure (NEXAFS or XANES) and electron energy-loss near-edge structures (ELNES) have been of broad interest for physicists, chemists, and materials scientists,<sup>1</sup> since they are sensitive to local electronic and geometric structures of selected atoms in a given compound or complex. On the absorption phenomenon, an electron is excited from a core level to an unoccupied orbital leaving a core hole. If the band structure remains rigid during the electronic transition, the partial density of unoccupied states (unoccupied PDOS), as a result of electric dipole selection rule, can be monitored using these spectroscopic techniques. However, the presence of the core hole sometimes changes the spectral shape from that of the ground-state unoccupied PDOS significantly: Sharp peaks that are not present in the ground-state PDOS are then observed near the absorption edge.<sup>2</sup> This is the so-called "core-hole effect" or "excitonic feature" on the absorption spectra.

The ground-state PDOS provides valuable information that is desired by many materials researchers, since it can be directly interpretable in terms of chemical environment of the selected element. However, the presence of the "core-hole effect" complicates the interpretation. The uncertainty for the magnitude of the "core-hole effect" eventually comprises a bottleneck for full use of the spectra for chemical analysis.

A number of experimental NEXAFS and ELNES studies have been made on alkali halides and some oxides. In these works extra features that did not coincide with the calculated PDOS at the ground state have been ascribed to be the "core-hole features." For example, O'Brien *et al.*<sup>3</sup> compared their NEXAFS spectra of MgO,  $\alpha$ -Al<sub>2</sub>O<sub>3</sub>, and MgAl<sub>2</sub>O<sub>4</sub> at the cation  $L_{23}$  edge with theoretical DOS. Their unoccupied DOS did not reproduce the experimental spectra; the origin of the major spectral features was concluded to be the atomlike excitons due to the presence of the core hole.

The influence of the core hole has been evaluated mainly through multiple-scattering calculations in which atoms are represented by a muffin-tin-shaped potential well. The

atomic number of the nucleus undergoing excitation is assumed to be increased by 1 in order to include the core-hole effects, which is called the  $Z+1$  approximation.<sup>4</sup> Although it is true that some of these multiple-scattering calculations successfully reproduced the experimental absorption spectrum, there are always uncertainties about the calculation associated with the non-self-consistency of the excited electron and arbitrary choice of the muffin-tin parameters. In addition, it is more useful for materials scientists to represent the excited electrons in terms of bands and bonds rather than scattered waves.

We have recently demonstrated that our first-principles molecular-orbital (MO) calculations for the ground state well reproduce all spectral features at the cation  $L_{23}$ -edge NEXAFS and ELNES of MgO and SiO<sub>2</sub> up to 30 eV.<sup>5-7</sup> The photoabsorption cross section (PACS) or oscillator strength for the transition as well as the unoccupied PDOS were calculated; they were found to be not significantly different. These results suggest that the presence of the core hole does not change the unoccupied PDOS features remarkably in these compounds at these edges. If this is the case, the experimental absorption spectra are directly interpretable through the comparison with the unoccupied PDOS, i.e., in terms of chemical bonding around the selected element as mentioned above.

In the present paper, we aim to understand the condition that should be satisfied to see a significant "core-hole effect," in other words, the limitation of using the ground-state PDOS for the interpretation of the experimental spectra. First-principles MO calculations are made for model clusters that include a core hole. The shape of the unoccupied PDOS at the ground state is compared with that at the intermediate state (Slater's transition state) and the final state of the transition. The results are discussed with special interest in the relationship between unoccupied MO structure that is determined by the chemical environment of atoms under investigation and the magnitude of the core-hole effect on the absorption spectra.

### COMPUTATIONAL PROCEDURES

Calculations were made for MgO,  $\alpha$ -Al<sub>2</sub>O<sub>3</sub> (corundum), and SiO<sub>2</sub> ( $\alpha$ -quartz) using model clusters of (Mg<sub>13</sub>O<sub>14</sub>)<sup>2-</sup>,

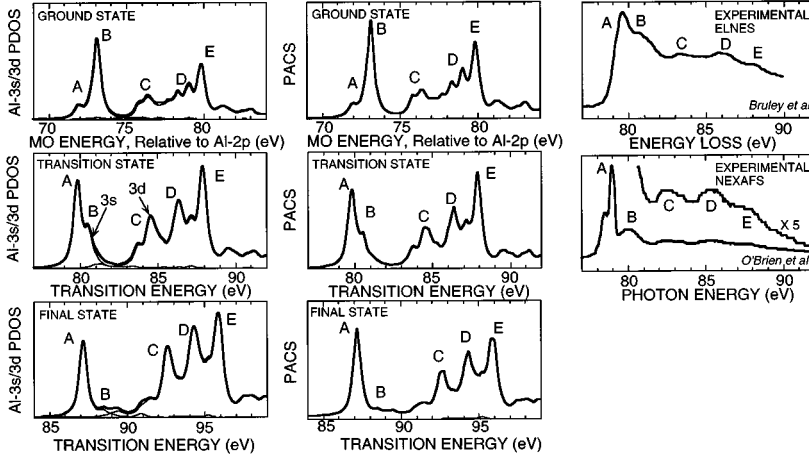


FIG. 1. Left: The sum of Al 3s and 3d unoccupied partial density of states (PDOS); middle: Al  $L_{23}$ -edge photoabsorption cross section (PACS) for  $\alpha$ -Al<sub>2</sub>O<sub>3</sub> using the (Al<sub>8</sub>O<sub>33</sub>)<sup>42-</sup> cluster at ground state (top), Slater's transition state (middle), and final-state electronic configuration (bottom). Right: Experimental spectra obtained by digitizing the reported curves in Refs. 3 and 13.

(Al<sub>8</sub>O<sub>33</sub>)<sup>42-</sup>, and (Si<sub>5</sub>O<sub>16</sub>)<sup>12-</sup>, respectively. They are cut from real crystals and embedded in a Madelung potential generated by point charges located at the external atomic sites. A cation atom is put at the center of the cluster, which is surrounded by one cation shell and two anion shells. The discrete-variational (DV)  $X\alpha$  method<sup>8,9</sup> is employed for the computation. In this method, a linear combination of numerically generated atomic orbitals given as follows is used to describe the MO's:

$$\phi_l(r_k) = \sum_i C_{il} \chi_i(r_k), \quad (1)$$

where  $\chi_i(r)$  denotes the atomic orbital (AO), and  $r_k$  is one of the sampling points in the DV calculation. All integrations are made in a numerical manner. Nearly minimal basis sets are used in order to clarify the simple relationship between spectral features and chemical bondings. Basis sets are 1s-2p for O and 1s-3d for Mg, Al, and Si. The numerical basis functions were obtained by solving the radial part of the Schrödinger equations. The radial part of the basis functions is thus flexible to chemical environment. Self-consistent calculations are made for three electronic configurations, namely, the ground state (initial state), the final state with the presence of a core hole, and Slater's transition state<sup>10</sup> in which a half electron is removed from the core orbital to fill an unoccupied orbital. The number of electrons in a cluster is the same for all three states. The total energy difference between the initial and the final states can be well approximated by the difference of one-electron orbital energies obtained for the Slater's transition state.<sup>10</sup>

The overlap population between the  $i$ th AO and the  $j$ th AO at the  $l$ th MO is given by

$$Q_{ij}^l = C_{il} C_{jl} \sum_k \omega(r_k) \chi_i(r_k) \chi_j(r_k), \quad (2)$$

where  $\omega(r_k)$  is the integration weight or reciprocal of the sample point density at  $r_k$ . The sum with respect to  $j$  provides the orbital population  $Q_i^l$  of  $i$ th AO at the  $l$ th MO, i.e.,

$$Q_i^l = \sum_j Q_{ij}^l. \quad (3)$$

The localization index for each MO,  $L_l$ , given by

$$L_l = \sum_i (Q_i^l)^2, \quad (4)$$

was computed in order to evaluate the spread of the  $l$ th MO among different atomic sites. The sum without squaring is unity, i.e.,

$$\sum_i Q_i^l = 1. \quad (5)$$

The definition of the localization index is the same as that used by Ching, Song, and Jaswal.<sup>11</sup> It has a value ranging from  $1/N$  to 1, where  $N$  is the total number of AO's,  $L_l$  is unity when the  $l$ th MO is perfectly localized and  $1/N$  when perfectly delocalized.

The oscillator strength  $I_{ij}$  for the electric dipole transition for photon absorption between states  $i$  and  $j$  is given by

$$I_{ij} = \frac{2}{3} \Delta E \langle j | \mathbf{r} | i \rangle|^2, \quad (6)$$

where  $\Delta E$  represents the transition energy. In the present work,  $I_{ij}$  is obtained directly by the numerical integration of the dipole matrix.<sup>12</sup>

## RESULTS AND DISCUSSION

The right-hand side of Fig. 1 compares the Al 2p edge ( $L_{23}$  edge) experimental ELNES by Bruley, Tseng, and Williams<sup>13</sup> and NEXAFS by O'Brien *et al.*<sup>3</sup> The two experimental spectra exhibit similar structures although the energy resolution is higher in the NEXAFS. The absolute loss energy is different by 0.6 eV; its reason is not clear. Splitting of the peak A is found only in the NEXAFS, which is attributable to the spin-orbit splitting components,  $2p_{3/2}$  and  $2p_{1/2}$ . The magnitude of the experimental splitting is 0.4 eV. This is in good agreement with the  $2p_{3/2}$ - $2p_{1/2}$  splitting for the free Al atom we have calculated using a relativistic Hartree-Fock-Slater method, that is 0.45 eV.

Calculations were made for three electronic configurations denoted by the ground state, transition state, and final state. Since the  $L_{23}$  absorption allowed lowest unoccupied MO (LUMO) in the (Al<sub>8</sub>O<sub>33</sub>)<sup>42-</sup> cluster is the 72a orbital, the electronic configuration for the transition state and the final state are taken to be  $(2p)^{5.5}(72a)^{0.5}$  and  $(2p)^{5.0}(72a)^{1.0}$ , respectively. The left and middle columns of

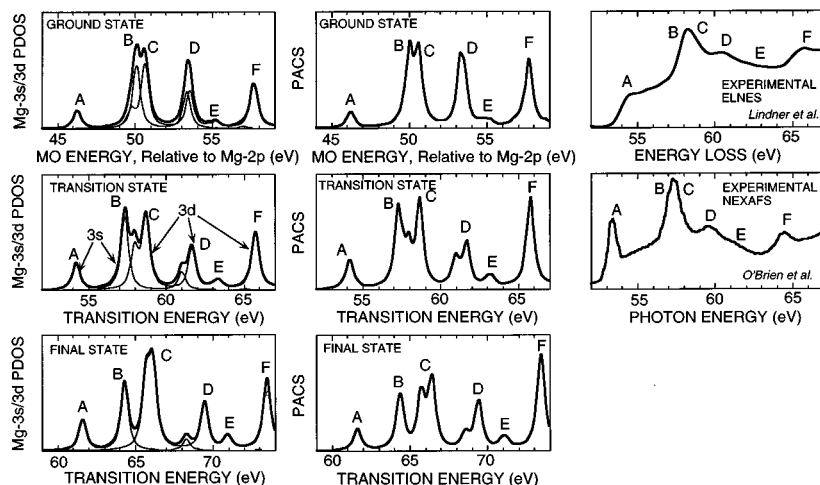


FIG. 2. Left: The sum of Mg 3s and 3d unoccupied PDOS; middle: Mg  $L_{23}$ -edge PACS for MgO using the  $(\text{Mg}_{13}\text{O}_{14})^{2-}$  cluster at ground state (top), Slater's transition state (middle), and final-state electronic configuration (bottom). Right: Experimental spectrum obtained by digitizing the reported curves in Refs. 3 and 15.

Fig. 1 compare the unoccupied PDOS and the Al  $L_{23}$ -edge theoretical PACS calculated for our  $\alpha\text{-Al}_2\text{O}_3$  cluster for three electronic configurations. Following the electric dipole selection rule, the cation  $2p$  core electron is excited to occupy the cation  $s$  and  $d$  unoccupied orbitals, which brings about the NEXAFS or ELNES at the cation  $L_{23}$  edge. Since we use a nearly minimal basis set throughout the present work for simplicity, a sum of Al 3s and 3d PDOS is shown as an approximation to the theoretical spectrum. The PDOS and PACS curves are made by broadening of discrete energy eigenvalues by a Lorentzian of 0.5 eV full width at half maximum. The energy separation between the  $2p$  core orbital and the  $72a$  orbital is used as the transition energy to the  $72a$  orbital, and the horizontal scale of the calculated spectra is translated. The sum of Al 3s and 3d PDOS and Al  $2p$  PACS are found to be almost the same. This fact confirms that the present PDOS is a good approximation of the theoretical PACS.

Both PDOS and PACS structures, especially the shape of the first peak near the edge, are found to be significantly dependent on the electronic configuration. Peak A, which is the low-energy shoulder of peak B at the ground state becomes the most prominent peak at the final state. It is also noticed that the separation between the first peaks (A, B) and the second peaks (C, D, and E) is dependent on the electronic configuration.

The intensity ratio of peaks A and B in the experimental spectra is best reproduced by the transition-state calculation. The ground-state calculation shows much smaller intensity of peak A than that of the experimental spectrum, and the final-state calculation exhibits much greater intensity of peak A. The three-peak feature of higher-energy peaks (C, D, and E) is well reproduced by the calculation irrespective of the electronic configuration. However, the energy separation between the first peaks (A, B) and the second peaks (C, D, and E) is larger by 1.5 eV in the theoretical spectrum at the transition state than the experimental spectrum. The small discrepancy seems to be general in the minimal basis-set calculations. As a matter of fact, Nakamatsu, Mukoyama, and Adachi<sup>14</sup> reported that the theoretical absorption spectrum by the DV- $X\alpha$  calculation overestimates the separation between individual features by a few percent when minimal

basis sets are used. However, the systematic discrepancy does not affect our peak assignments at all. Peaks A and B originate from Al 3s orbitals and C, D, and E are ascribed to Al 3d orbitals. The absolute transition energy obtained by the present transition-state calculation overestimates the experimental NEXAFS by 0.9 eV at the peak A. When spin polarization during the transition<sup>7</sup> is taken into account, the transition energy decreased by 1.0 eV, and the theoretical value shows excellent agreement with the experimental one.

Similar calculations were conducted for a model cluster of MgO, and the results are compared with the experimental ELNES by Lindner *et al.*<sup>15</sup> and NEXAFS by O'Brien *et al.*<sup>3</sup> in Fig. 2. For the  $(\text{Mg}_{13}\text{O}_{14})^{2-}$  cluster in  $O_h$  symmetry, the  $L_{23}$  absorption allowed LUMO is  $12a_{1g}$ . Therefore,  $(2p)^{5.5}(12a_{1g})^{0.5}$  and  $(2p)^{5.0}(12a_{1g})^{1.0}$  configurations were used for the transition-state and final-state calculations. The presence of the core hole does not change the shape of the first peak in the Mg  $L_{23}$ -edge spectrum contrary to the case of the Al  $L_{23}$ -edge spectrum of  $\alpha\text{-Al}_2\text{O}_3$ . Only the splitting of the second peak that is denoted by B and C increases when the core hole is present. As a result, the experimental spectrum can be reproduced even by the ground-state calculation as reported previously.<sup>5</sup> The absolute transition energy of peak A obtained at the transition state is only 1 eV greater than that of the experimental spectrum. The agreement between the ground-state spectrum and the experimental cation  $L_{23}$ -edge XANES is similarly good for  $\text{SiO}_2$  ( $\alpha$ -quartz). We have reported that the theoretical Si  $L_{23}$ -edge PACS is not significantly modified by the presence of a Si  $2p$  core hole.<sup>7</sup>

Since Al is located between Mg and Si in the periodic table, the exceptional photoabsorption spectrum of  $\alpha\text{-Al}_2\text{O}_3$  at the Al  $L_{23}$  edge cannot be explained simply by the nature of the Al atom itself. We have to consider the environment of the excited atom in detail. Because all of these compounds are typical insulators having fully oxidized cations, their primary bonding mechanisms are the same. However, small differences in their chemical environment may change the excited-state structures notably.

Contour maps of the LUMO's in the  $(\text{Al}_8\text{O}_{33})^{42-}$  and the  $(\text{Mg}_{13}\text{O}_{14})^{2-}$  clusters, i.e.,  $72a$  and  $12a_{1g}$ , at three electronic configurations are shown in Fig. 3. These MO's are responsible for the peak A in the experimental spectra. At the ground state, these MO's are mainly composed of a cation

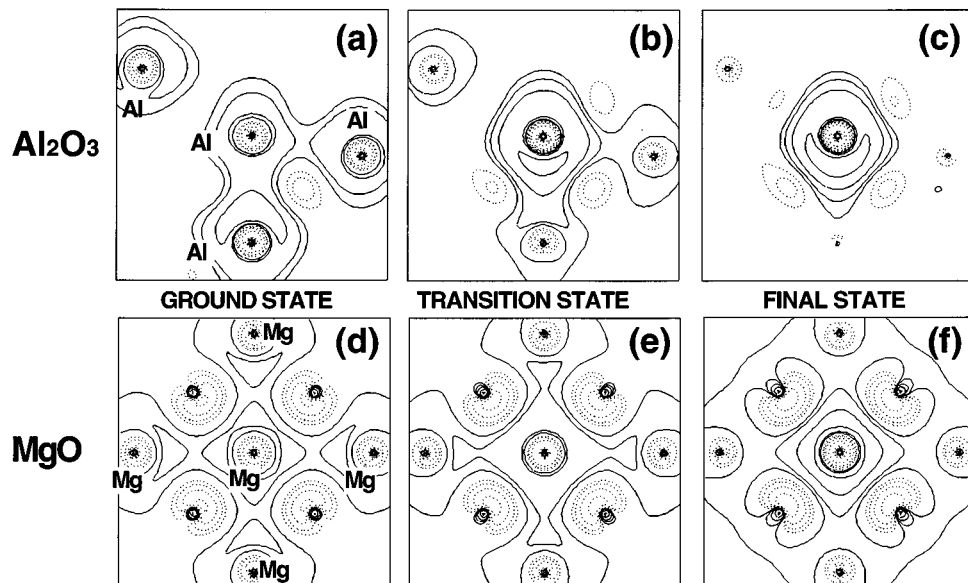


FIG. 3. (a) Contour map of the  $72a$  orbital in the  $(\text{Al}_8\text{O}_{33})^{42-}$  cluster at the initial state, (b) at the transition state, and (c) at the final-state electronic configuration. (d) The  $12a_{1g}$  orbital in the  $(\text{Mg}_{13}\text{O}_{14})^{2-}$  cluster at the initial state, (e) at the transition state, and (f) at the final state. Curves are drawn for  $\pm 0.016$ ,  $\pm 0.032$ ,  $\pm 0.064$ ,  $\pm 0.128$ ,  $\pm 0.256$ , and  $\pm 0.512$ , respectively. Broken curves are for negative values.

$3s$  orbital overlapping with its neighboring cation  $3s$  orbitals. On the formation of a core hole, the nuclear potential is temporarily deepened. As a result, electrons tend to be bound to the nucleus. As can be seen from Fig. 3, the magnitude of the localization is more significant in  $\alpha\text{-Al}_2\text{O}_3$  than in MgO. The  $72a$  orbital in the  $(\text{Al}_8\text{O}_{33})^{42-}$  cluster almost localizes at the Al atom undergoing excitation at the final state. The localization of  $12a_{1g}$  orbital in the  $(\text{Mg}_{13}\text{O}_{14})^{2-}$  cluster is much weaker even at the final state. The magnitude of the localization can be quantified by the localization index of these MO's. The values for three configurations are displayed in Fig. 4. Significant localization of the  $72a$  orbital of the  $(\text{Al}_8\text{O}_{33})^{42-}$  cluster during the transition process can be

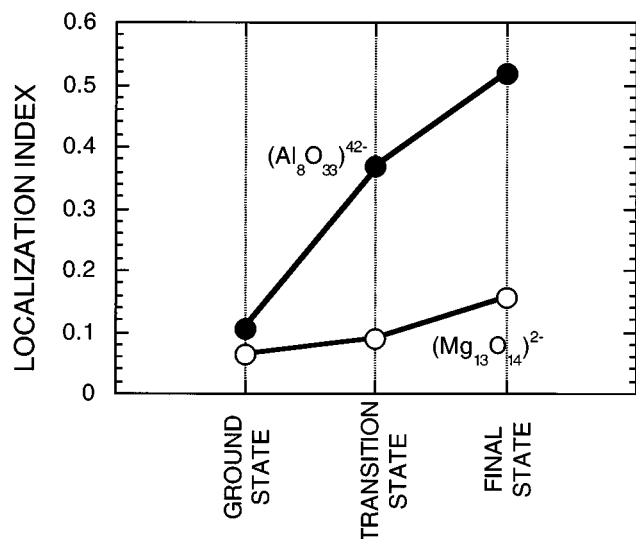


FIG. 4. Localization index of  $72a$  orbital in the  $(\text{Al}_8\text{O}_{33})^{42-}$  cluster and  $12a_{1g}$  orbital in the  $(\text{Mg}_{13}\text{O}_{14})^{2-}$  cluster at the initial, transition, and final states.

seen. This is the phenomenological origin of the notable core-hole feature in  $\alpha\text{-Al}_2\text{O}_3$  near the Al  $L_{23}$  edge.

The magnitude of the localization due to the formation of the core hole is expected to be greater when the overlap between neighboring cation AO's is stronger. The overlap population between the neighboring cation orbitals for the LUMO at the ground-state configuration is calculated and shown in Table I together with the corresponding cation-cation distances. The overlap population between the neighboring cation orbitals is found exceptionally strong only for one special Al-Al bond in  $\alpha\text{-Al}_2\text{O}_3$ : It is 0.2653 nm, which is about 10–20% shorter than the other cation-cation bonds in the other two compounds. It is natural to expect that the overlap of cation orbitals is strong only for this particular bond. As a matter of fact, the localization associated with the formation of the core hole occurs significantly only in  $\alpha\text{-Al}_2\text{O}_3$  near the Al  $L_{23}$  edge.

The spatial distribution of unoccupied MO's responsible for the higher-energy peaks is greater in general. These MO's interact with more atoms than those responsible for near-edge peaks discussed in the present paper. The relationship between atomic arrangements and the magnitude of

TABLE I. Cation-cation bond lengths, coordination numbers, and calculated overlap populations at the  $L_{23}$  absorption allowed LUMO for three compounds.

	Cation-cation	
	Bond length (nm) and coordination number	Overlap population
MgO	$0.2978 \times 12$	0.055
$\alpha\text{-Al}_2\text{O}_3$	$0.2653 \times 1$	0.142
	$0.2792 \times 3$	0.046
	$0.3223 \times 3$	0.008
$\text{SiO}_2$ ( $\alpha$ -quartz)	$0.3061 \times 4$	0.043

core-hole features may therefore be more difficult to understand intuitively.

In summary, the cation  $L_{23}$ -edge X-ray-absorption spectra of three oxides are found to be well reproduced by the first-principles molecular-orbital calculations using model clusters composed of a cation atom with one cation shell and two oxygen shells. A core hole is included in the self-consistent calculation. The strongest peak that appears in the spectrum of  $\alpha$ - $\text{Al}_2\text{O}_3$  is found to be due to the presence of an Al  $2p$

core hole. The origin of the significant core-hole excitonic feature in  $\alpha$ - $\text{Al}_2\text{O}_3$  is ascribed to the presence of an exceptionally short Al-Al bond in the  $\alpha$ - $\text{Al}_2\text{O}_3$  structure, which brings about strong overlap of the neighboring cation orbitals.

This work was supported by Grant-in-Aid for General Scientific Research from Ministry of Education, Sports, Science and Culture of Japan.

- 
- <sup>1</sup>J. Stöhr, *NEXAFS Spectroscopy* (Springer, Berlin, 1992); *Transmission Electron Energy Loss Spectrometry in Materials Science*, edited by M. M. Disco, C. C. Ahn, and B. Fultz (TMS, Warrendale, 1992).
- <sup>2</sup>S. T. Pantelides, *Phys. Rev. B* **11**, 2391 (1975), and references therein.
- <sup>3</sup>W. L. O'Brien, J. Jia, Q-Y. Dong, T. A. Callcott, D. R. Mueller, D. L. Ederer, and C-C. Kao, *Phys. Rev. B* **47**, 15 482 (1993).
- <sup>4</sup>T. Fujikawa, *J. Phys. Soc. Jpn.* **52**, 4001 (1983).
- <sup>5</sup>I. Tanaka, J. Kawai, and H. Adachi, *Solid State Commun.* **93**, 553 (1995).
- <sup>6</sup>I. Tanaka, J. Kawai, and H. Adachi, *Phys. Rev. B* **52**, 11 733 (1995).
- <sup>7</sup>I. Tanaka and H. Adachi, *J. Phys. D.* (to be published).
- <sup>8</sup>H. Adachi, M. Tsukada, and C. Satoko, *J. Phys. Soc. Jpn.* **45**, 875 (1978).
- <sup>9</sup>D. E. Ellis, H. Adachi, and F. W. Averill, *Surf. Sci.* **58**, 497 (1976).
- <sup>10</sup>J. C. Slater, *Quantum Theory of Molecules and Solids* (McGraw-Hill, New York, 1974).
- <sup>11</sup>W. Y. Ching, L. W. Song, and S. S. Jaswal, *Phys. Rev. B* **30**, 544 (1984).
- <sup>12</sup>H. Adachi and K. Taniguchi, *J. Phys. Soc. Jpn.* **49**, 1944 (1980).
- <sup>13</sup>J. Bruley, M-W. Tseng, and D. B. Williams, *Microsc. Microanal. Microstruct.* **6**, 1 (1995).
- <sup>14</sup>H. Nakamatsu, T. Mukoyama, and H. Adachi, *J. Chem. Phys.* **95**, 3167 (1991).
- <sup>15</sup>T. Lindner, H. Sauer, W. Engel, and K. Kambe, *Phys. Rev. B* **33**, 22 (1986).